Energy coupling of membrane transport and efficiency of sucrose dissimilation in yeast

Henderson, Ryan K.; de Valk, Sophie C.; Poolman, Bert; Mans, Robert

DOI
10.1016/j.ymben.2020.11.014

Publication date
2020

Document Version
Final published version

Published in
Metabolic Engineering

Metabolic Engineering xxx (xxxx) xxx

Contents lists available at ScienceDirect

Metabolic Engineering

journal homepage: www.elsevier.com/locate/meteng

Energy coupling of membrane transport and efficiency of sucrose dissimilation in yeast

Ryan K. Henderson [a,1], Sophie C. de Valk [b,1], Bert Poolman [a,**], Robert Mans [b,*]

[a] Department of Biochemistry, University of Groningen, Nijenborgh 4, 9747, AG Groningen, the Netherlands
[b] Department of Biotechnology, Delft University of Technology, Van der Maasweg 9, 2629, HZ Delft, the Netherlands

ARTICLE INFO

Keywords:
Membrane transport
Energy coupling
Directed evolution
Microbial bioenergetics
Sucrose
Chemostat
ATP
Substrate uptake

ABSTRACT

Proton coupled transport of α-glucosides via Mal11 into *Saccharomyces cerevisiae* costs one ATP per imported molecule. Targeted mutation of all three acidic residues in the active site resulted in sugar uniport, but expression of these mutant transporters in yeast did not enable growth on sucrose. We then isolated six unique transporter variants of these mutants by directed evolution of yeast for growth on sucrose. In three variants, new acidic residues emerged near the active site that restored proton-coupled sucrose transport, whereas the other evolved transporters still catalysed sucrose uniport. The localization of mutations and transport properties of the mutants enabled us to propose a mechanistic model of proton-coupled sugar transport by Mal11. Cultivation of yeast strains expressing one of the sucrose uniporters in anaerobic, sucrose-limited chemostat cultures indicated an increase in the efficiency of sucrose dissimilation by 21% when additional changes in strain physiology were taken into account. We thus show that a combination of directed and evolutionary engineering results in more energy efficient sucrose transport, as a starting point to engineer yeast strains with increased yields for industrially relevant products.

1. Introduction

In heterotrophic microorganisms, an important determinant of the maximal product yield is the amount of energy (ATP) conserved by substrate dissimilation and the energy requirements of assimilatory reactions, as this coupling determines the distribution of substrate over biomass and product formation. Therefore, the energy metabolism in microbial production hosts is an important optimization target to obtain high product yields, which is essential for the production of bulk chemicals where the carbon feedstock can make up 70% of the total variable costs of industrial processes (de Kok et al., 2012; Borodina and Nielsen, 2014; Pfromm et al., 2010). An increase of the energetic efficiency of substrate dissimilation could decrease the costly oxygen demand of compounds whose formation require the input of ATP (like biomass, proteins or complex chemicals) or even enable anaerobic production of compounds with an ATP neutral production pathway, such as lactic acid in engineered *S. cerevisiae* strains (van Maris et al., 2004).

Metabolic engineering strategies have been developed to increase energetic efficiency, for instance by altering the route for cytosolic acetyl-CoA supply and increasing the efficiency of the respiratory chain and the H^+-ATPase (de Kok et al., 2012). In the yeast *Saccharomyces cerevisiae*, it has previously been shown that the ATP yield of dissimilation of the disaccharides maltose and sucrose could be increased by substituting intracellular hydrolysis by phosphorolysis (de Kok, 2011; Marques, 2018a). Whereas transport of monosaccharides occurs predominantly through uniport, all known disaccharide transporters are proton-coupled symporters belonging to the Major Facilitator Superfamily (MFS) (Horák, 2013; Serrano, 1977; Van Leeuwen et al., 1992). As proton export via the plasma membrane ATPase comes at a net cost of 1 ATP per proton in *S. cerevisiae*, the energetic efficiency of these engineered strains did not exceed that of regular glucose metabolism. For the complete conversion of extracellular substrate to extracellular product, energetic requirements for substrate import and/or product export can be a major contributor to the total energy costs. In an attempt to increase the ATP yield of sucrose dissimilation, the expression of a sucrose phosphorylase was combined with expression of a heterologous transporter from *Phaseolus vulgaris* (PvSuf1), that was described to facilitate

* Corresponding author.
** Corresponding author.
E-mail addresses: b.poolman@rug.nl (B. Poolman), r.mans@tudelft.nl (R. Mans).
[1] Shared-first authorship.

https://doi.org/10.1016/j.ymben.2020.11.014
Received 11 July 2020; Received in revised form 4 November 2020; Accepted 30 November 2020
Available online 3 December 2020

sucrose uniport (Marques et al., 2018a). However, the experimental data indicated that, in contrast to what was suggested in previous research (Zhou et al., 2007), the transport of sucrose by PvSuf1 in *S. cerevisiae* was (at least partially) proton coupled.

In *S. cerevisiae*, The α-glucoside transporter Mal11 catalyses proton-coupled import of a wide range of sugars into *S. cerevisiae*, including maltose, sucrose and maltotriose (Serrano, 1977; Van Leeuwen et al., 1992; Han et al., 1995; Stambuk and de Araujo, 2001; Pao et al., 1998; Yan, 2015) and has been an engineering target to modulate cellular energetics (Basso et al., 2011). The acidic residues involved in proton coupling in Mal11 are Glu-120, Asp-123 and Glu-167 (Henderson and Poolman, 2017). Mutation of one or two of these acidic residues to neutral residues created a "leak" pathway in the transport cycle (Pao et al., 1998), which allowed some of the sugar substrate to be transported in the absence of a proton (Lolkema and Poolman, 1995; Henderson et al., 2019). Mutation of all three residues completely abolished proton-coupled transport but still enabled facilitated diffusion of the substrate.

In this work, we investigated the ability of uncoupled Glu-120/Asp-123/Glu-167 triple Mal11 mutants to enable growth of *S. cerevisiae* in medium containing sucrose as the sole carbon source. Parallel directed evolution experiments were then applied to acquire a series of second-site suppressor mutations, which were able to restore the transport function of the mutated Mal11 transporters. We found that for some of the evolved acidic residue mutants proton coupling was restored, whereas the other transporters still catalysed sugar uniport. We characterized the physiology of reverse-engineered strains expressing the evolved mutated sucrose transporters in sucrose-limited anaerobic chemostats to investigate the impact of the mutations in Mal11 on the energetic efficiency of sucrose dissimilation. In addition, the properties

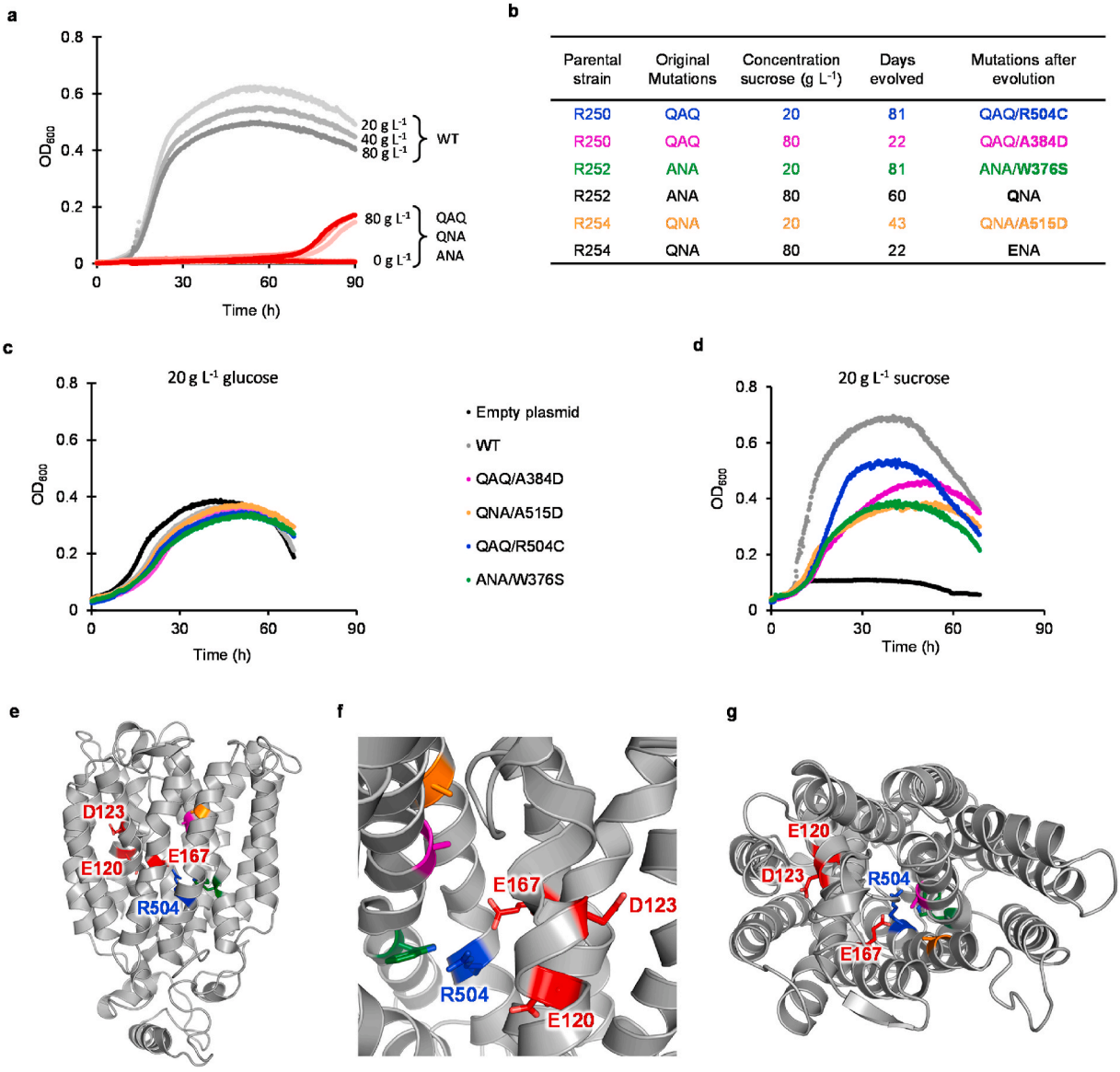

Parental strain	Original Mutations	Concentration sucrose (g L^{-1})	Days evolved	Mutations after evolution
R250	QAQ	20	81	QAQ/R504C
R250	QAQ	80	22	QAQ/A384D
R252	ANA	20	81	ANA/W376S
R252	ANA	80	60	QNA
R254	QNA	20	43	QNA/A515D
R254	QNA	80	22	ENA

Fig. 1. Directed evolution of triple Mal11 mutants. **a**: Growth of unevolved IMZ630 strains expressing wildtype or triple mutated versions of Mal11 in 96-well plates with SC containing 0, 20, 40 or 80 g L^{-1} sucrose as sole carbon source. For each strain, one representative dataset of two independent experiments is shown. **b**: Mutations that occurred in Mal11 during directed evolution of Mal11 triple mutants. Strains were grown on the indicated sucrose concentrations until rapid growth occurred. Strains that could rapidly grow on 80 g L^{-1} sucrose were transferred to 20 g L^{-1} sucrose until rapid growth resumed. Mutations that were not present in the unevolved parental strain are represented in bold. **c, d**: Growth of IMZ630 strains expressing evolved versions of Mal11 in 96-well plates with SC containing 20 g L^{-1} glucose (**c**) or 20 g L^{-1} sucrose (**d**). For each strain, one representative dataset of two independent experiments is shown. **e, f, g**: Structural model of Mal11(Henderson and Poolman, 2017) highlighting the location of the introduced mutations and the evolved mutation R504C during construction and directed evolution of triple mutants on sucrose. The locations of other evolved mutations are shown in Supplementary Fig. S4.

of the identified mutations and corresponding transporter variants were used to propose a model of the transport mechanism of Mal11, which has the potential to be applied for the design of targeted engineering strategies to change the mechanism of other MFS transporters.

2. Results

2.1. Mal11 triple mutants are unable to facilitate rapid growth on sucrose

Previously constructed Mal11 triple mutant transport proteins were able to catalyse rapid, coupled or uncoupled maltose transport in radiolabelled sugar transport assays (Henderson and Poolman, 2017). To study the transport of sucrose by these mutated Mal11 proteins *in vivo*, wildtype Mal11 and the three variants Glu-120-Gln/Asp-123-Ala/Glu-167-Gln ($Mal11_{QAQ}$), Glu-120-Ala/Asp-123Asn/Glu-167-Ala ($Mal11_{ANA}$), and Glu-120-Gln/Asp-123-Asn/Glu-167-Ala ($Mal11_{QNA}$) were expressed in *S. cerevisiae* strain IMZ630 using episomal plasmids. IMZ630 carries deletions of genes encoding all native disaccharide transporters and hydrolysis enzymes (suc^-) and overexpresses an integrated copy of sucrose phosphorylase from *Leuconostoc mesenteroides* (LmSPase) (Marques et al., 2018a). We then tested the ability of the resulting strains to grow aerobically in medium containing 20, 40 or 80 g L^{-1} sucrose as the sole carbon source using YNB medium in 96-well plates. Within 30 h, growth of the strain expressing wildtype Mal11 was observed in each of the cultures, whereas none of the triple mutants grew in media containing 20 or 40 g L^{-1} sucrose after 90 h. However, in the cultures containing 80 g L^{-1} sucrose, the triple mutants exhibited growth after three days (Fig. 1a).

2.2. Second-site suppressor mutations enable faster growth on sucrose

Next, we evolved the yeast strains carrying the three triple mutants by selecting for faster growth on sucrose, using sequential batch cultivation in shake flasks with synthetic complete media (SC) and 80 g L^{-1} sucrose as the sole carbon source (Mans et al., 2018). When the cultures with 80 g L^{-1} sucrose were able to reach a high cell density within 2–3 days after dilution, they were transferred to SC medium with 20 g L^{-1} sucrose for further evolution. Within three months, all six evolution cultures were able to grow within two days in medium with 20 g L^{-1} sucrose. Single colonies were then isolated and the evolved *MAL11* genes were amplified and sequenced (Fig. 1b).

The *MAL11* expression plasmids were purified from the evolved single colonies and introduced into the unevolved IMZ630 (suc^-, LmSPase) background. All strains displayed wildtype-like growth in medium containing 20 g L^{-1} glucose (Fig. 1c) and were able to grow well on medium containing 20 g L^{-1} sucrose (Fig. 1d), showing that the suppressor mutations in Mal11 are responsible for the gain of function.

Mapping of the additional mutations that arose during evolution onto a homology model of Mal11 (Henderson and Poolman, 2017) uncovered that, although the two residues Ala-384-Asp (TM7) and Ala-515-Asp (TM11) are located on different helices, they are both found in the central cavity of the protein, on helix faces oriented inwardly, and are at the same height along the transport pathway. Importantly, they are also all in close proximity to the three mutated acidic residues E120 (TM1), D123 (TM1), and E167 (TM4) (Supplementary Fig. S4): Using E167 as a central reference point, the distance to A384 and A515 are 7.6 Å and 9.7 Å, respectively. The other two mutations, Arg-504-Cys (TM11) and Trp-376-Ser (TM7), are located at the bottom of the central cavity, on adjacent helices in the structure, facing inwardly, and are at the same height along the transport pathway (Fig. 1e–g, Supplementary Fig. S4). Notably, Arg-504 is the only basic residue in the transmembrane region of Mal11 and is the only charged residue remaining in the central cavity of the uncoupled triple mutants.

2.3. Coupling mechanism of evolved Mal11 mutants

To investigate whether the additional mutations altered the transport mechanism of the mutants, each Mal11 protein was tagged with fluorescent YPet and overexpressed in strain IMK291, using the inducible *GAL1* promotor on a multicopy plasmid. IMK291 lacks all native disaccharide transporters and hydrolysis enzymes (suc^-) and has been used previously to study the mechanism of disaccharide transport (Marques et al., 2018a). Visualisation of galactose-induced cells with fluorescence microscopy showed that all Mal11-YPet variants are properly localised to the periphery of the cell (Fig. 2a). Flow cytometry analysis indicated a roughly five-fold lower average fluorescence intensity of the fluorescent population of $Mal11_{QNA/A515D}$ compared to wildtype Mal11 (Supplementary Fig. S1). Apparently, the A515D mutation destabilized the Mal11 protein resulting in increased turnover in the yeast plasma membrane.

Next, the ability of the IMK291-derived strains for substrate uptake in the presence 1 mM radiolabelled maltose or sucrose was tested and the ratio between intra- and extracellular sugar concentrations (accumulation ratio) was determined. The results indicate that the transporters that evolved a new acidic residue in the central cavity ($Mal11_{QAQ/A384D}$ and $Mal11_{QNA/A515D}$) could accumulate both sugars inside the cell (accumulation ratio >1), suggesting a restored proton-coupled transport mechanism (Fig. 2b). The second group of mutants ($Mal11_{QAQ/R504C}$ and $Mal11_{ANA/W376S}$) could not accumulate either sugar within 45 min, which could be an indication of a very low transport rate at low substrate concentrations or energy-independent sugar import. From each group of mutants, the initial rates of transport of the Mal11 mutants derived from a fast-growing strain ($Mal11_{QAQ/R504C}$ and $Mal11_{QNA/A515D}$) (Fig. 1d) at a range of sucrose concentrations were compared to that of their corresponding unevolved triple mutant. Transport measurements with ≥50 mM sucrose were obscured by the background signal, and therefore kinetic parameters K_m and V_{max} could not be estimated. However, important trends are visible in the data obtained at lower sucrose concentrations. While at 1 mM sucrose there was little difference in the initial rates between the strains expressing no Mal11 (negative control), $Mal11_{QAQ}$ and $Mal11_{QAQ/R504C}$, at 20 mM sucrose, the rate of transport of strains expressing $Mal11_{QAQ/R504C}$ (0.069 ± 0.016 nmol 10^{-6} cells min^{-1}) was six-fold faster (p-value < 0.05) than that of $Mal11_{QAQ}$ (0.011 ± 0.012 nmol 10^{-6} cells min^{-1}) (Fig. 2c). The increased uptake rate of sucrose at higher concentrations is most likely the result of the selection for mutants able to catalyse fast transport under high-substrate conditions. Similarly, initial transport rates of strains expressing unevolved $Mal11_{QNA}$ were low compared to those of strains expressing $Mal11_{QNA/A515D}$ (Fig. 2d).

2.4. Consequences of uncoupled transport on cellular energetics

Strains in which sucrose transport is proton coupled require subsequent extrusion of the proton via the H^+-ATPase, resulting in a net expense of 1 ATP per transported sucrose (Fig. 3a). To analyse the effect of the energy coupling mechanism on cellular energetics and strain physiology, a fast-growing uncoupled mutant, R270 ($Mal11_{QAQ/R504C}$) and proton-coupled mutant, R267 ($Mal11_{QNA/A515D}$) (Fig. 1d) were selected for further analysis with respect to their impact on the energetic efficiency of sucrose dissimilation. For this purpose, the strains are preferentially grown under anaerobic conditions, where the theoretical difference in the energetic efficiency of sucrose dissimilation between sucrose-proton symport and uniport would be 25% (increase from 4 ATP to 5 ATP per sucrose) and result in a 25% increased biomass yield.

To avoid growth-rate dependent effects, the strains were characterized in anaerobic steady-state chemostat cultures. In the preceding batch phase, the maximum specific growth rates were 0.33 ± 0.00 h^{-1} for R249 (wildtype Mal11), 0.09 ± 0.00 h^{-1} for R270 ($Mal11_{QAQ/R504C}$) and 0.17 ± 0.00 h^{-1} for R267 ($Mal11_{QNA/A515D}$) (Supplementary Fig. S2). Based on these growth rates, we decided to operate the chemostats at a constant dilution rate of 0.07 h^{-1} and samples were taken once steady state conditions were reached. In steady state, the biomass yield of R270 ($Mal11_{QAQ/R504C}$) was 0.095 ± 0.002 g biomass g $sucrose^{-1}$, which is

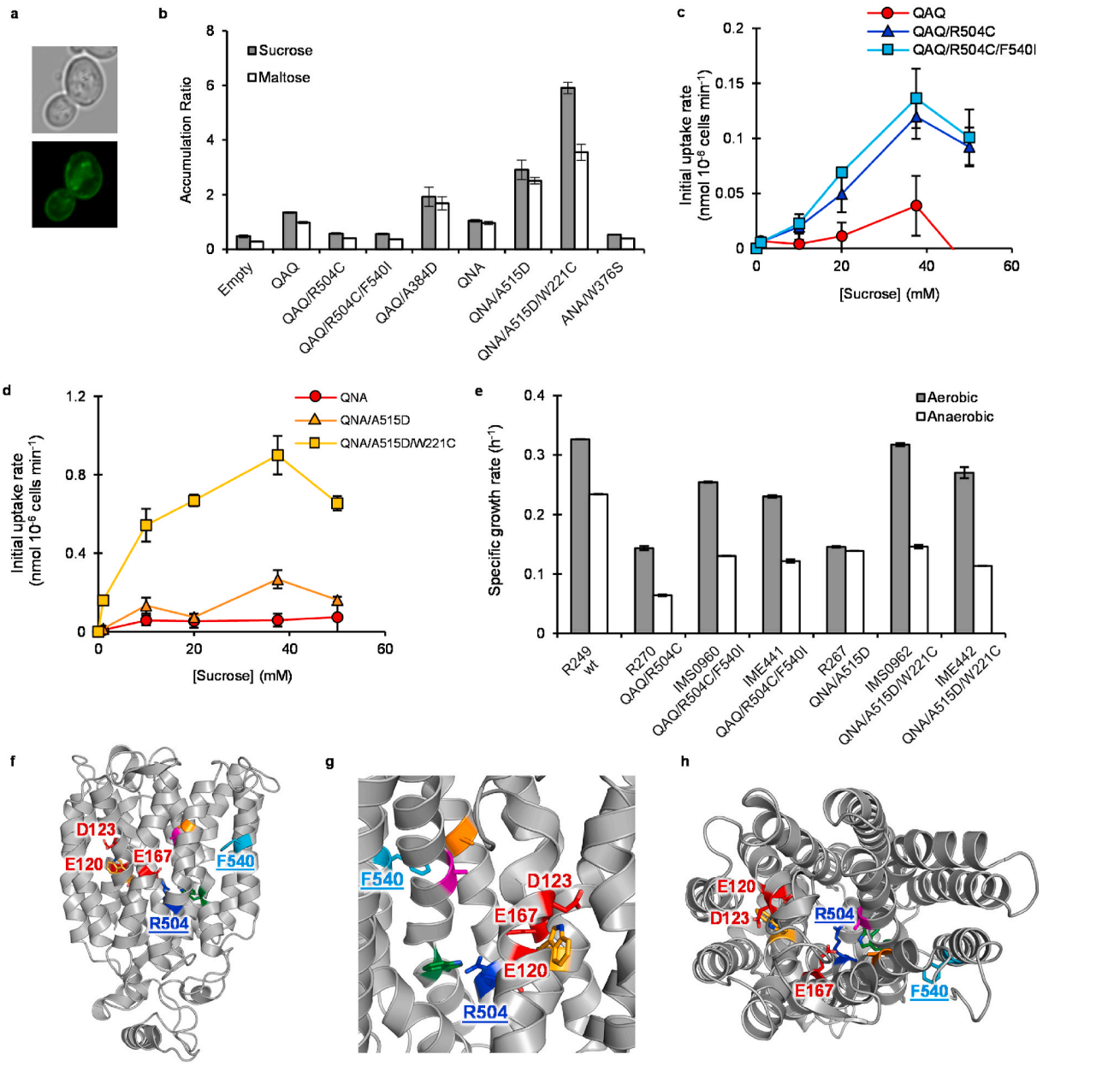

Fig. 2. Transport characteristics of evolved and unevolved Mal11 triple mutants. a: Representative confocal fluorescence microscopy image of IMK291 strains expressing wildtype and mutant Mal11-Ypet from the *GAL1* promoter on pRHA00L-based plasmids, including brightfield (top) and fluorescence (bottom) image. b: Uptake of 1 mM ^{14}C-maltose and 1 mM ^{14}C-sucrose after 30 min. Bars and error bars represent the average and standard deviation, respectively, of triplicate measurements. c, d: Concentration dependence of sucrose transport by unevolved and evolved Mal11 transporters. Cells were equilibrated at 30 °C for 10 min before addition of 1, 5, 25, 37.5, and 50 mM ^{14}C-sucrose. After 1 or 2 min of incubation, cells were filtered and the amount of intracellular radioactivity was determined to calculate the initial transport rate. Points and error bars represent the background-subtracted average and standard deviation, respectively, of triplicate measurements. e: Aerobic and anaerobic specific growth rates of strains carrying variants of Mal11, including single colony isolates from anaerobic chemostats (IMS0960 and IMS0962) and their corresponding reverse engineered strains (IME441 and IME442) in shake flasks containing SM with 20 g L^{-1} sucrose. Growth rates were calculated from optical density measurements from at least five data points in the exponential phase. Data represent average values and mean deviations of duplicate experiments. f, g, h: Structural model of Mal11 (Henderson and Poolman, 2017) highlighting the location of the introduced and evolved mutations of the QAQ/R504C/F540I mutant. A structural model with the location of mutations in QNA/A515D/W221C is shown in Supplementary Fig. S5.

~9% higher (p-value = 0.09) than that of the reference strain R249 (Mal11, 0.087 ± 0.002 g biomass g^{-1} sucrose). Surprisingly, the biomass yield of R267 (Mal11$_{QNA/A515D}$, 0.060 g g^{-1} sucrose) was ~31% lower than that of R249 (Fig. 3b). These apparent differences in energetic efficiency are reflected in the biomass specific rates of sucrose uptake and ethanol plus CO_2 production, as the energetic efficiency of sugar dissimilation dictates the rate of sucrose dissimilation to ethanol and CO_2 to provide ATP for biomass formation at identical growth rates. Overall, the data suggest that the energetic efficiency of R270 (Mal11$_{QAQ/R504C}$) is increased and that of R267 (Mal11$_{QNA/A515D}$) is decreased compared to R249 (wildtype Mal11).

We then investigated the basis for the lower than expected increase in biomass yield (9 versus 25%) of R270. To this end, we first determined the extracellular concentration of glucose-1-phosphate, which could be formed when sucrose phosphorylase (LmSPase) is released from the cells. Extracellular sucrose phosphorolysis would lead to extracellular glucose-1-phosphate accumulation and fructose uptake, resulting in an overall yield of only 2 ATP per sucrose (Fig. 3a). High

a

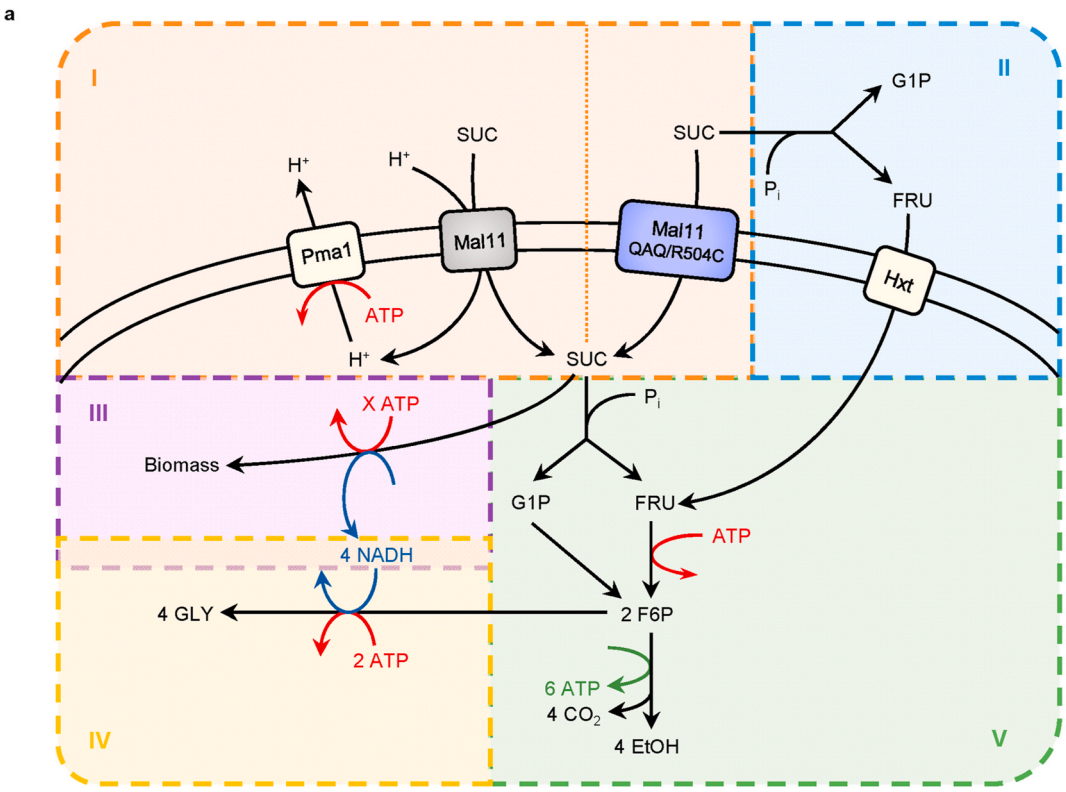

b

Strain	R249	R270	R267
Mal11	Wildtype	QAQ/R504C	QNA/A515D
Biomass yield (g_x $g_{sucrose}^{-1}$)	0.087 ± 0.002	0.095 ± 0.002	0.060 ± 0.001
$q_{sucrose}$ (mmol g_x^{-1} h^{-1})	-2.41 ± 0.01	-2.17 ± 0.01	-3.33 ± 0.01
$q_{ethanol}$ (mmol g_x^{-1} h^{-1})	7.51 ± 0.33	6.22 ± 0.13	10.9 ± 0.04
q_{CO2} (mmol g_x^{-1} h^{-1})	8.32 ± 0.38	6.92 ± 0.09	11.3 ± 0.04
$q_{glycerol}$ (mmol g_x^{-1} h^{-1})	0.56 ± 0.03	0.78 ± 0.07	0.77 ± 0.01
Residual sucrose (g L^{-1})	0.06 ± 0.01	5.68 ± 0.06	1.99 ± 0.00
Protein content (g g_x^{-1})	0.46 ± 0.01	0.50 ± 0.01	0.48 ± 0.01
Glucose-1-phosphate (mM)	0.007 ± 0.00	2.04 ± 0.09	0.82 ± 0.07

c

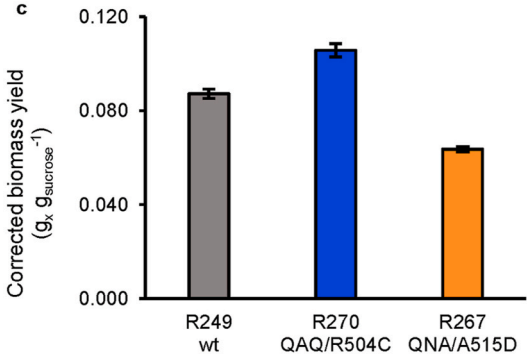

Fig. 3. Energetic efficiency of sucrose metabolism. a: Schematic representation of sucrose metabolism in R249, R270 and R267. I: Proton-coupled sucrose transport requires the expense of one ATP per sucrose for extrusion of the co-transported proton by Pma1. II: Extracellular sucrose phosphorylase activity leads to extracellular formation of G1P, which cannot be imported, and fructose, imported by Hxt transporters, resulting in an overall yield of 2 ATP per sucrose. III: Biomass formation requires biomass-composition-dependent investment of ATP. IV: Glycerol formation to re-oxidize NADH from biosynthesis requires sucrose for carbon (0.25 mol SUC mol GLY^{-1}) and ATP (depending on SUC transport mechanism, either 1 or 0.75 mol ATP mol GLY^{-1}). V: Intracellular sucrose dissimilation to ethanol by sucrose phosphorylase and glycolysis, yielding 5 ATP per sucrose. SUC = sucrose, FRU = fructose, G1P = glucose-1-phosphate, F6P = Fructose-6-phosphate, GLY = glycerol, EtOH = ethanol. b: Growth characteristics of R249, R270 and R267 in sucrose-limited anaerobic chemostat cultures at a dilution rate of 0.07 h^{-1}. Biomass specific production and consumption rates are depicted as $q_{metabolite}$. The data represent average values and mean deviations obtained from duplicate experiments. c: Biomass yields after correction for 1) increased glycerol production, 2) extracellular sucrose phosphorylase and 3) increased protein content. R249 (wt Mal11) was used as reference for the corrections, hence the corrected biomass yield of this strain is identical to the measured biomass yield. Bars and error bars represent the average and mean deviations of the corrected biomass yields calculated for each duplicate experiment.

glucose-1-phosphate concentrations were measured in the cultures of R270 ($Mal11_{QAQ/R504C}$, 2.04 ± 0.09 mM) and R267 ($Mal11_{QNA/A515D}$, 0.82 ± 0.07 mM) but were negligible for R249 (wildtype Mal11) (Fig. 3b). Most likely, the higher residual sucrose concentrations observed for R270 and R267 compared to R249 (Fig. 3b) allowed for the increased extracellular sucrose phosphorolysis rate.

Next, we quantified the effect of increased glycerol formation on the biomass yield. In anaerobic *S. cerevisiae* cultures, glycerol is formed to re-oxidize NADH generated in biosynthetic reactions (van Dijken and Scheffers, 1986). We found that the biomass specific glycerol production rates of both R267 and R270 are ~38% higher than for the reference strain (Fig. 3b). Formation of glycerol from sucrose requires the investment of substrate in the form of carbon as well as energy (Fig. 3a), and therefore negatively affects the biomass yield. Furthermore, the increased specific glycerol production rate at identical growth rates indicates an increased oxidation state of the biomass and a change in biomass composition. Since the protein fraction of biomass accounts for the majority of the energetic costs of biosynthesis, we determined the protein content in each of the steady-state chemostat cultures. We found that the protein content of R270 (0.50 ± 0.01 g g^{-1} biomass) and R267 (0.48 ± 0.01 g g^{-1} biomass) were increased by 10 and 5% relative to R249 (0.46 ± 0.01 g g^{-1} biomass) (Fig. 3b). This suggests that on top of

extracellular sucrose phosphorolysis and increased glycerol formation, R270 and R267, carrying engineered Mal11, also have an increased energetic cost of biomass formation.

2.5. Additional mutations in Mal11 enable fast anaerobic growth

In the anaerobic pre-cultures grown on sucrose used to inoculate the bioreactors, we observed a ~90 h lag phase prior to exponential growth of strain R267 ($Mal11_{QNA/A515D}$) (data not shown), which prompted us to search for additional mutations in the *MAL11* gene of strains grown in anaerobic chemostat cultures and sampled at the end of the experiment. In addition to the four mutations in Mal11 that were initially present, R270 had gained a Phe-540-Ile mutation ($Mal11_{QAQ/R504C/F540I}$) and R267 had gained a Trp-221-Cys mutation ($Mal11_{QNA/A515D/W221C}$). Single colonies of these double-evolved cultures of R270 and R267 were isolated and named IMS0960 and IMS0962, respectively. When tested under aerobic conditions, the specific growth rates of both IMS0960 ($0.25 \pm 0.00\ h^{-1}$) and IMS0962 ($0.32 \pm 0.00\ h^{-1}$) were higher than the parental strains R270 ($0.14 \pm 0.00\ h^{-1}$) and R267 ($0.15 \pm 0.00\ h^{-1}$) (Fig. 2e). Under anaerobic conditions, the growth rate of IMS0960 ($Mal11_{QAQ/R504C/F540I}$) was also higher ($0.13 \pm 0.00\ h^{-1}$) than its parent R270 ($0.06 \pm 0.00\ h^{-1}$), whereas the growth rates of IMS0962 ($0.15 \pm 0.00\ h^{-1}$) and R267 ($0.14 \pm 0.00\ h^{-1}$) were similar.

Next, the *MAL11*-carrying plasmids of IMS0960 and IMS0962 were introduced into the unevolved background strain IMZ630 and the growth rates under aerobic and anaerobic conditions were determined (Fig. 2e). From the observed growth rates, it is evident that the F540I mutation in *MAL11* is solely responsible for the higher aerobic and anaerobic growth rate of IMS0960, whereas the W221C mutation decreased the lag phase in IMS0962 (Supplementary Fig. S3). Most likely, IMS0962 contains another (genomic) mutation responsible for the increased anaerobic growth rate compared to IME442.

To examine whether the additional F540I and W221C mutations changed the transport mechanism, $Mal11_{QAQ/R504C/F540I}$ and $Mal11_{QNA/A515D/W221C}$ were also expressed in IMK291 and the ability of the resulting strains to accumulate maltose or sucrose was investigated using radiolabelled substrates (Fig. 2b). $Mal11_{QNA/A515D/W221C}$ was able to accumulate both sugars and no sugar accumulation was observed in the strains expressing $Mal11_{QAQ/R504C/F540I}$, which indicates that the transport mechanism of both transporters was not altered by the acquisition of the fifth mutation. The initial transport rates of $Mal11_{QAQ/R504C/F540I}$ at 1 and 20 mM sucrose were comparable to that of $Mal11_{QAQ/R504C}$ (Fig. 2c), whereas the W221C mutation improved the transport rates compared to $Mal11_{QNA/A515D}$ (Fig. 2d). Flow cytometry analysis indicated that unlike $Mal11_{QNA/A515D}$, the average fluorescence intensity of the fluorescent population expressing $Mal11_{QNA/A515D/W221C}$ was similar to that of the mutants (Supplementary Fig. S1). Apparently, the W221C mutation resolved the issue of Mal11 protein expression or instability in the membrane that resulted from the A515D mutation. The increased influx of sucrose by this stabilized Mal11 variant could also explain the reduced lag phase when cells are transferred from aerobic to anaerobic conditions. A low expression level would not be expected to affect steady-state accumulation levels of sucrose in the IMK291 background but would impact initial uptake rates, which is in accordance with the results shown in Fig. 2d.

3. Discussion

In previous work, the proton relay network of Mal11 consisting of Glu-120, Asp-123, and Glu-167 was studied and mutants with an uncoupled transport mechanism were characterized (Henderson and Poolman, 2017). Here, we have expanded on that work by discovering a number of second-site suppressor mutations in Mal11 required for efficient growth of *S. cerevisiae* on sucrose. We identified three suppressor mutants that regained sugar-proton symport activity and two mutants that were still uncoupled. The effect of one coupled and one uncoupled variant of Mal11 on the energetic efficiency of yeast was investigated in anaerobic chemostats. We show that proton-decoupled transport of sucrose allows this yeast to dissimilate sucrose in an energetically more efficient way, but the engineered proteins come with additional phenotypic effects, resulting in an altered biomass composition and extracellular metabolite profile.

3.1. Suppressor analysis yields two classes of mutants

Analysis of second-site suppressors arising from evolution studies is a powerful tool for biochemists to study the relationship between protein sequence and function and has a long history of use in transporters, because structural information is directly linked to functional data (Arastu-Kapur et al., 2005; Pi et al., 2002; Saraceni-Richards and Levy, 2000; Pazdernik et al., 1997; Jessen-Marshall et al., 1997). The evolution experiment under aerobic conditions gave rise to two types of mutants. One type contained mutations in which a new acidic residue replaced a neutral residue in the upper portion of the central cavity (A384D, A515D) and in the other type a mutation to a residue below the binding site occurred (W376S, R504C) (Fig. 1b, e-g). The new acidic aspartate residues in the evolved transporters are all located one helix-turn above Glu-167, at the top of the central cavity (Fig. 1e–g), and all three Mal11 variants are capable of active sucrose uptake (Fig. 2b). Apparently, proton coupling in the uncoupled triple mutants can be restored via the introduction of a single acidic residue in the vicinity of the sugar-binding cavity and there is flexibility in terms of the exact position of the residue.

The second class of mutants (W376S, R504C) hints at a cytoplasmic gate of the transporter that alternately seals and opens the central cavity from the cytoplasm and thereby controls the release of substrate, a molecular mechanism previously suggested for Major Facilitator Superfamily transporters based on the amassed body of crystal structures (Quistgaard et al., 2016). Such a gate could potentially involve Arg-504, which is located in close proximity to Glu-167 at the bottom of the central cavity.

3.2. Modelling of the data: class I mutants

Based on the localization and transport properties of the acidic residue mutants and the evolved second-site suppressors, we propose a model of proton-coupled sugar transport by Mal11 (Fig. 4a). Although there is insufficient evidence to suggest whether sugar and proton binding is ordered, we propose the following mechanism: Glu-167 becomes protonated and sugar binds to outward-facing Mal11 and induces closure of the extracellular gate; Arg-504 is then released from the interdomain salt-bridge with Glu-167 and is free to swing away from the transport path to interact with Trp-376, opening the cytoplasmic side of the protein; the inward-facing transporter then releases the sugar and proton, at which point Glu-167 and Arg-504 are available for interaction with each other and the inward-to-outward switch is once again permitted.

This model can be used to explain the phenotypes of the *S. cerevisiae* strains expressing mutated transporters. The unevolved triple mutants lack Glu-167, meaning no salt bridge can form with Arg-504, which makes the outward-facing conformation less favourable compared to the inward-facing state (Fig. 4b). With the conformational probability shifted towards the inward-facing state, there is an unchanged or increased likelihood of sugar binding at the intracellular face of Mal11. Such a mechanism explains why the triple mutants have slow sugar influx (Fig. 2c and d) but demonstrate wildtype-like efflux and exchange (Henderson and Poolman, 2017).

The evolved Asp residues one helix-turn above Gln- or Ala-167 may serve to facilitate closure of the extracellular gate upon substrate binding and may even bind substrate due to their position at the top of the central cavity (Fig. 4c). Arg-504 is likely too far away from the evolved Asp for salt-bridge formation, so the outward-facing conformation

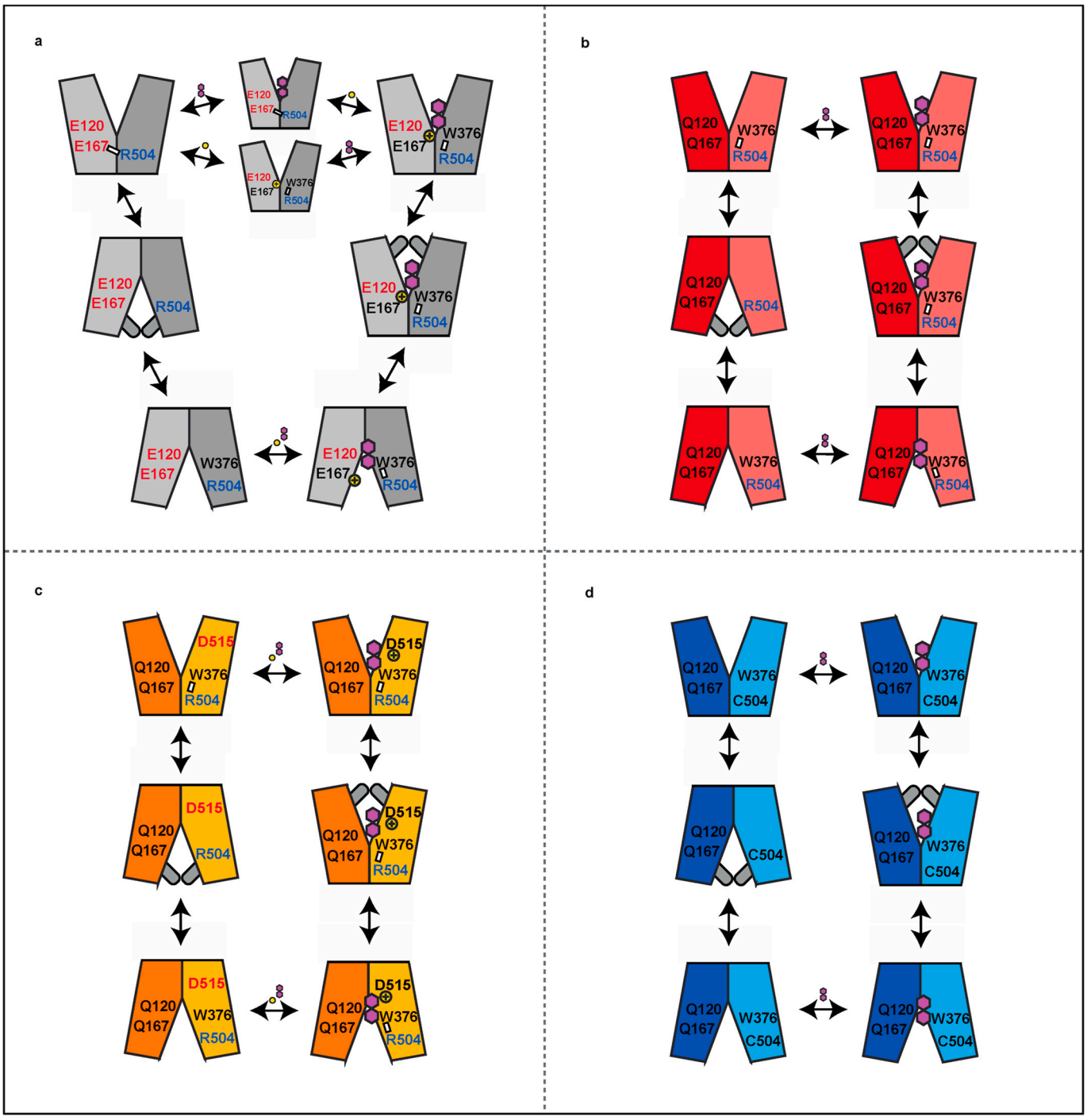

Fig. 4. Model of proton-coupled transport by Mal11. a: In the wildtype transporter, the cycle of conformational changes is regulated by the alternate interactions of Arg-504 with Glu-167 or Trp-376. In the outward-facing conformation, binding of a proton (yellow circle) to Glu-167 releases Arg-504 and permits interaction with Trp-376. Binding of sugar (pink hexagons) causes the extracellular gate to close around the substrate. With both sugar and proton bound, the transporter switches to an inward-facing conformation and releases its substrates before returning to an outward-facing conformation. b: In the triple mutant transporters (only $Mal11_{QAQ}$ is shown), the salt-bridge between Glu-167 and Arg-504 can no longer form, and without transmembrane acidic residues the transporters are no longer proton-coupled. Thus, only sugar is transported via uniport. c: In the triple mutants with an evolved aspartate residue ($Mal11_{QAQ/A384D}$, and $Mal11_{QNA/A515D}$), the acidic residue facilitates closure of the extracellular gate of the protein. This makes the conformational transitions occur more rapidly than in the triple mutants. However, with the evolution of a central cavity acidic residue comes (partial) restoration of proton-coupled transport. d: The evolved triple mutants with a mutation at the bottom of the central cavity ($Mal11_{QAQ/R504C}$ and $Mal11_{ANA/W376S}$; only $Mal11_{QAQ/R504C}$ is shown), both interactions (Glu-167 with Arg-504 and Trp-376 with Arg-504) governing proton-coupled conformational changes are disrupted and thus conformational changes may be more flexible. Without a protonatable residue in the central cavity, proton binding cannot occur and thus the transporter is uncoupled, as in the triple mutants. (For interpretation of the references to colour in this figure legend, the reader is referred to the Web version of this article.)

remains unfavourable compared to the wildtype. Protonation and interaction of the evolved acidic residue with the substrate would stabilize the outward-facing conformation and promote closure of the top of the transporter.

Protonation-based closure of the transporter would provide a mechanism for leaky proton coupling and may even create an EH-leak (proton leak) pathway (Lolkema and Poolman, 1995; Henderson et al., 2019). In a cellular context, such a proton leak pathway would result in a net energetic cost of 1 ATP per proton and could contribute to the low biomass yield of R267 ($Mal11_{QNA/A515D}$), which was ~31% lower than the well coupled wildtype Mal11-expressing strain R249 (Fig. 3b). The anaerobic cultivation of R267 led to mutation of a central cavity residue, W221C. An isogenic population carrying this additional mutation (IMS0961) exhibited a ~79% reduced lag phase under anaerobic conditions (Supplementary Fig. S3). From fluorescence measurements of YPet-tagged constructs, the W221C mutation appeared to vastly increase the protein abundance level of transporter in the membrane (Supplementary Fig. S1) and doubled the accumulation level of the sugar (Fig. 2b). The additional mutation may play a predominantly structural, rather than catalytic, role.

3.3. Modelling of the data: class II mutants

In the second class of evolved mutants ($Mal11_{QAQ/R504C}$ and $Mal11_{ANA/W376S}$), both interactions that mediate proton coupling in the wildtype transporter have been disrupted (Fig. 4d). Without the interaction between Arg-504 and Trp-376, the inward-facing conformation becomes less favourable than in the unevolved triple mutants, which increases the likelihood of the outward-facing conformation. This could result in an increased opportunity for extracellular sucrose binding and transport in Mal11 variants unable to bind and transport protons, due to a lack of acidic residues in the central cavity. Sucrose uptake studies indicated that both $Mal11_{QAQ/R504C}$ and $Mal11_{ANA/W376S}$ appear to be fully uncoupled (Fig. 2b) and behave as sugar uniporters, which is in accordance with the transport model presented here.

After anaerobic cultivation, an additional mutation arose, F540I, which was located at a helix-helix interface away from the central cavity. While this mutation did not have any distinct effect on the accumulation level (Fig. 2b), initial transport rates (Fig. 2c) or expression level (Supplementary Fig. S1), the *S. cerevisiae* strain expressing $Mal11_{QAQ/R504C/F540I}$ grew significantly faster than the $Mal11_{QAQ/R504C}$ mutant (Fig. 2e). We speculate that the F540I mutation may have increased the protein stability (less protein turnover), therefore resulting in improved overall growth performance.

3.4. Biomass yield and energetic efficiency

Expression of the uncoupled $Mal11_{QAQ/R504C}$ in a sucrose phosphorylase expressing strain was expected to result in a 25% increase in biomass yield compared to a strain expressing the proton-coupled wildtype Mal11, corresponding to an increase in energetic efficiency of 4–5 ATP per sucrose (Marques et al., 2018a). However, in steady-state chemostat cultures the biomass yield of R270 ($Mal11_{QAQ/R504C}$) was increased by only 9% ($p = 0.09$) compared to the reference strain (wildtype Mal11). Three possible contributors to this lower-than-expected biomass yield were identified: (i) increased extracellular sucrose phosphorolysis; (ii) increased specific glycerol formation rates; and (iii) an increased biomass protein content (Fig. 3a). The increased glycerol production is most likely linked to the increased protein content, as synthesis of amino acids from sugars is the major NADH yielding process in *S. cerevisiae* cells (Verduyn et al., 1990).

To determine whether these observed effects could fully explain the low yield, we estimated the biomass yields that would have been achieved by R270 if it would display a similar growth phenotype as the control strain R249 (wildtype Mal11) (see Biomass yield calculations in Material and methods section). With these assumptions, the 'corrected' biomass yield of R270 would be 0.106 ± 0.03 g g^{-1} sucrose, which is a $21.3 \pm 2.9\%$ increase relative to R249 and close to the predicted value of 25% (p-value < 0.05) (Fig. 3c). A fourth factor that could explain the remaining 5% is increased cellular maintenance due to increased protein turnover as a result of a higher protein content (van Bodegom, 2007; Canelas et al., 2010; Hong et al., 2012). Finally, we cannot rule out the possibility that proton-leakage through the uncoupled $Mal11_{QAQ/R504C}$ transporter causes additional consumption of ATP, and thus lead to a lower biomass yield in this strain.

3.5. Application of engineered transporters for industrial strains

The data and analysis of energy coupling mechanisms in metabolite transport presented in this work can be applied for future design of other energy-efficient transporters to improve product yields and volumetric productivity in the biotechnological industry. When we account for increased glycerol formation, extracellular phosphorolysis of sucrose and a change in biomass composition, $Mal11_{QAQ/R504C}$ has increased the energetic efficiency of sucrose dissimilation by 21%. For industrial application of this engineered transporter, the aforementioned factors that limit its beneficial impact on final product yields will have to be addressed. Although we have not identified clear metabolic engineering targets to resolve the increased protein content, glycerol production and extracellular phosphorolysis, we propose a directed evolution strategy for further optimization of yeast strains expressing $Mal11_{QAQ/R504C}$ as a next step. To avoid the emergence of new acidic residues that restore proton coupling, it is essential that a selective pressure on ATP-independent sucrose transport is maintained. Since combined use of a sucrose uniporter and phosphorylase theoretically increases the ATP yield of anaerobic sucrose dissimilation (to ethanol) to 2.5 ATP per hexose equivalent, which is higher than the 2 ATP obtained from anaerobic dissimilation of glucose, a strain design resulting in a 'zero ATP pathway' on glucose could be used to enable such an evolutionary strategy. This strategy could for example be achieved in an engineered homofermentative lactic acid producing *S. cerevisiae* strain, where the conversion of sucrose to lactic acid only conserves ATP when energy-independent sucrose transport is maintained (van Maris et al., 2004).

The design and construction of yeast strains able to catalyse energetically efficient uptake and conversion of polysaccharides has the potential to improve industrial production of energy requiring (anabolic) products. Furthermore, by exceeding the energetic efficiency (per hexose equivalent) of glucose utilization, energy efficient polysaccharide utilization could also enable anaerobic production of products whose biosynthetic pathway from glucose does not provide ATP for cellular maintenance and growth (van Maris et al., 2004; Zelle et al., 2008; van Rossum et al., 2016). While we focussed on sucrose, an important industrial sugar predominantly derived from sugarcane (Marques et al., 2015), we hypothesize that our proposed model could be applied in the design of improved cell factories on other carbon substrates. For example, for other oligosaccharides, such as maltose, cellobiose, trehalose, cellodextrin and lactose, phosphorylases have already been described (de Kok et al., 2011; Alexander, 1968; Belocopitow and Maréchal, 1970; de Groeve et al., 2009; Sheth and Alexander, 1967; Sadie et al., 2011), whereas a uniporter has only been described for cellobiose (Kim et al., 2014). In addition, even when future research leads to the identification of additional polysaccharide uniporters in other organisms, expression of heterologous transporters in microbial cell factories remains a significant challenge (Marques et al., 2018a, 2018b). Therefore, a combination of rational engineering, for which our model could act as a starting point, and evolutionary engineering of endogenous transporters could be a valuable alternative strategy to obtain improved transporters. For example, de Kok et al. (2011) proposed a strategy for trisaccharide utilization which could yield even more ATP per hexose unit (2.67 ATP), requiring a maltotriose uniporter and a maltose and maltotriose phosphorylase (de Kok et al., 2011). While a maltotriose uniporter has thus far not been identified in nature,

a recent evolution study revealed that a maltotriose transporter could evolve by combination of multiple maltose transporters in *Saccharomyces eubayanus* (Brouwers et al., 2018). Since the resulting chimeric transporter has a high sequence similarity to *S. cerevisiae MAL11,* our evolved $Mal11_{QAQ/R504C}$ transporter provides valuable insights that can be applied to engineer the coupling mechanism of the chimeric maltotriose transporter.

In conclusion: We show that proton coupling in sugar transport by Mal11 requires a single acidic residue but the protein tolerates various locations for these residues around the sugar-binding site. On the basis of our mutant analysis and functional studies, and building on previous structural studies, we propose a model for energy coupling in the *S. cerevisiae* Mal11 disaccharide transporter. Furthermore, we demonstrate that a combination of targeted protein engineering and subsequent evolutionary engineering results in a sucrose facilitator, as a starting point to engineer energy-efficient yeast strains with increased yields of industrially relevant products.

4. Material and methods

4.1. Strains and maintenance

All *S. cerevisiae* strains used in this study (Supplementary Table S1) are derived from the CEN.PK lineage (Entian and Kötter, 2007; Salazar et al., 2017) and *Escherichia coli* strains MC1061 and XL1 blue were used to store and amplify plasmids. To prepare stock cultures, glycerol was added to growing cultures to a final concentration of 30% (v/v) and 1 mL aliquots were stored at −80 °C. *S. cerevisiae* transformations were performed as described previously (Gietz and Woods, 2002) using 1 μg of DNA, unless specified otherwise. All plasmids and their sources and primers are listed in Supplementary Tables 2 and 3

4.2. Media and cultivation

E. coli was cultivated in LB medium, using 100 μg/mL ampicillin for selection and maintenance of plasmids. *S. cerevisiae* strains were cultivated in YPD (1% (w/v) yeast extract, 2% (w/v) peptone, 2% (w/v) glucose, pH 6.0), in synthetic complete media (SC) (0.67% (w/v) yeast nitrogen base without amino acids) (YNB, Formedium, UK) or synthetic medium (SM) (pH 6.0 when used in shake flasks) prepared as described previously (Pazdernik et al., 1997). When needed, SC was supplemented with a Kaiser amino acid mixture lacking leucine, uracil, or both (Formedium, UK). For growth characterization in shake flasks, SM with 2.3 g L^{-1} urea (pH 6.0) as the sole nitrogen source was used (Luttik et al., 2000). SM used in bioreactors was supplemented with autoclaved (20 min at 121 °C) Antifoam Emulsion C to a final concentration of 0.2 g L^{-1}.

Aerobic shake flask cultures were grown in an Innova incubator shaker at 30 °C and 200 rpm using 500 mL round-bottom shake flasks containing 100 mL medium. Anaerobic shake flask cultures were grown at 30 °C in a Bactron anaerobic chamber with an atmosphere of 5% (v/v) H_2, 6% (v/v) CO_2 and 89% (v/v) N_2, on a IKA KS 260 basic shaker at 200 rpm, using 50 mL shake flasks containing 30 mL medium.

Bioreactor cultivations were performed in 2-L laboratory bioreactors (Applikon Biotechnology, Delft, The Netherlands) with a working volume of 1 L. Cultures were stirred at 800 rpm and sparged with 500 mL N_2/min (<5 ppm O_2). The medium vessels were sparged with N_2 as well. The pH of the culture was maintained at 5.0 by automated addition of 2 M KOH and the temperature was controlled at 30 °C. The reactors were inoculated with *S. cerevisiae* strains to obtain an initial optical density (OD_{660}) of approximately 0.15. After the batch phase, the medium pump was switched on to obtain a constant flowrate. The working volume was kept constant using an effluent pump controlled by an electric level sensor. Chemostat cultures were assumed to be in steady state when, after five volume changes, the culture dry weight, extracellular concentrations of sucrose, ethanol and glycerol and CO_2 production rate varied by less than 2% over at least 2 more volume changes. At the end of each experiment, the actual dilution rate and carbon recovery were determined (Supplementary Table S4).

For plate-based growth assays, *S. cerevisiae* strains cultivated for at least two days in SC with 1% (v/v) ethanol to an OD_{600} of roughly 0.5. Cells were then diluted in 1× SC to an OD_{600} between 0.1 and 0.4, and, subsequently, the cells were dispensed in 60 μL aliquots into microplate wells and mixed with 30 μL of 2× SC plus 30 μL of 2× carbon source. 96-well flat-bottom microplates (CELLSTAR, Greiner Bio-One) were used and sealed with a Breath-Easy membrane (Sigma-Aldrich). OD_{600} measurements were made at 10 min intervals using a PowerWave 340 spectrophotometer (BioTek) and cells were maintained at 30 °C with shaking at variable speed in between measurements. All growth assays included blank wells (SC and carbon source) for each carbon source, the values of which were subtracted from all measurements as background.

4.3. Directed evolution of Mal11 triple mutants

S. cerevisiae strains R250 ($Mal11_{QAQ}$), R252 ($Mal11_{ANA}$), and R254 ($Mal11_{QNA}$) were grown on SD/-AA and each diluted to an OD_{600} of 0.1 in 50 mL SCM containing 2% (w/v) and 8% (w/v) sucrose in 250 mL flasks. When an OD_{600} greater than 1 was reached, the culture was diluted in fresh media to an OD_{600} of 0.1. This process was repeated at least two more times for each culture until the time between dilutions was 24–48 h, at which point samples were sequenced and glycerol stocks were made. Evolution lines growing rapidly in SCM with 8% (w/v) sucrose were then diluted in 50 mL SCM with 2% (w/v) sucrose and the above evolution protocol was repeated.

Evolved plasmids from single colonies were isolated and transformed into *E. coli* for amplification and then sequencing of *MAL11*. These plasmids were subsequently introduced into IMZ630, resulting in strains R265 ($Mal11_{QAQ/A384D}$), R267 ($Mal11_{QNA/A515D}$), R270 ($Mal11_{QAQ/R504C}$) and R274 ($Mal11_{ANA/W376S}$).

At the end of the chemostat cultures single colonies were isolated, resulting in IMS0960 (evolved R270) and IMS0962 (evolved R267). From both single cell lines, plasmids were isolated, renamed pUDE862 (from IMS0960) and pUDE864 (from IMS0962) and introduced into IMZ630, resulting in IME441 and IME442, respectively.

4.4. Analytical methods

Growth was monitored by optical density (OD) measurement at a wavelength of 660 nm. For biomass dry weight measurements, 10 mL culture was filtered over a pre-weighed nitrocellulose filter with pore size 0.45 μm. Subsequently, the filters were washed with demineralized water and dried for 20 min at 360 W in a microwave oven, after which they were weighed again. Concentrations of sucrose, ethanol and glycerol in culture supernatants were measured via HPLC analysis on an Agilent 1260 HPLC, equipped with a Bio-Rad HPX 87H column. Detection was performed by means of an Agilent refractive index detector and an Agilent 1260 VWD detector. Off-gas concentrations of CO_2 and O_2 were measured using an NGA 2000 analyzer.

Glucose-1-phosphate concentrations in culture supernatant were enzymatically determined by measuring the reduction of $NADP^+$ by glucose-6-phosphate dehydrogenase before and after addition of phosphoglucomutase. Cellular protein content was determined as described previously (Verduyn et al., 1990) with the exception that 1 M NaOH was used instead of 1 M KOH and the absorbance was measured at 510 nm instead of 550 nm.

4.5. Transport assays using radiolabelled sugars

Sugar transport was measured in whole yeast cells essentially as previously described (Henderson and Poolman, 2017). *S. cerevisiae* strains were pre-cultured on SE/-AA or SE/-Leu, as appropriate, before harvesting in early exponential phase of growth by centrifugation at 3000 g for 5 min at 4 °C. After washing twice in 3 mL assay buffer

(potassium-citrate-phosphate (KCP) + 10 mM galactose), cells were resuspended in assay buffer and stored on ice for no more than 4 h. Initially, cells at an OD_{600} of 12 or 24 were incubated for 10 min at 30 °C to increase the adenylate energy charge (Guimarães and Londesborough, 2008), followed by addition of approximately 48,100 Bq/mL [U–^{14}C]maltose or [U–^{14}C]sucrose (both 600 mCi/mmol; American Radiolabeled Chemicals, Inc.) to start the reaction. Measurements were taken by addition of a reaction sample to 2 mL ice-cold KCP and rapid filtration on 0.45 μm pore-size cellulose-nitrate filters (GE-Healthcare, Little Chalfont, UK), which were pre-soaked in KCP plus 1 mM sugar. Filters were then washed with an additional 2 mL KCP, dissolved in 2 mL scintillation solution (Emulsifier^{plus}, PerkinElmer, Waltham, MA, USA), and the radioactivity quantified in a Tri-Carb 2800 TR liquid scintillation analyzer (PerkinElmer). The amount of intracellular maltose or sucrose was normalized to 10^6 cells by counting the number of cells in samples of 20 μL at OD_{600} of 0.4 in an Accuri C6 flow cytometer (BD Biosciences, Durham, USA). The intracellular concentration of sugar was calculated using an estimated 60 fL internal volume per cell. Purity of radiolabeled substrates was checked by TLC and generally better than 99%, aliquots were stored in the freezer and used within one year.

4.6. Statistical analysis

Mean values and mean deviations were calculated from the data obtained from two independent experiments. Significance was assessed by performing a two-sided unpaired Student's t-test. Differences were considered to be significant if a p-value < 0.05 was obtained.

5. Biomass yield calculations

5.1. Glycerol formation

Differences in biomass specific glycerol production rates ($\Delta q_{glycerol}$, in mol g_x^{-1} h^{-1}) between reference strain R249 (wt Mal11) and R270 ($Mal11_{QAQ/R504C}$) or R267 ($Mal11_{QNA/A515D}$) (Fig. 3b) were used to calculate the effect on the steady-state concentration of glycerol ($\Delta C_{glycerol}$, in mol l^{-1}) for a reactor with biomass concentration C_x (in g_x l^{-1}) and dilution rate D (in h^{-1}) via Equation (1):

$$\Delta C_{glycerol} = \frac{\Delta q_{glycerol} \cdot C_x}{D} \quad (1)$$

Biosynthesis of 1 mol glycerol requires 0.25 mol sucrose and 0.75 mol ATP (Fig. 3a). For R270 ($Mal11_{QAQ/R504C}$) sucrose uniport was assumed (Fig. 2b), resulting in 5 mol ATP formed in anaerobic dissimilation of 1 mol sucrose. Therefore, sucrose consumed by R270 for additional glycerol formation ($\Delta C_{s,glycerol}^{R270}$ in mol l^{-1}) was calculated via Equation (2):

$$\Delta C_{s,glycerol^{R270}} = 0.25^* \Delta C_{glycerol} + 0.75^*0.2^* \Delta C_{glycerol} \quad (2)$$

For R267 ($Mal11_{QNA/A515D}$) sucrose proton symport was assumed (Fig. 2b), resulting in the requirement of an additional 0.25 mol ATP per glycerol and 4 ATP formed in anaerobic dissimilation of 1 mol sucrose. Sucrose consumed by R267 for additional glycerol formation ($\Delta C_{s,glycerol}^{R267}$) was calculated via Equation (3):

$$\Delta C_{s,glycerol^{R267}} = 0.25^* \Delta C_{glycerol} + 1^*0.25^* \Delta C_{glycerol} \quad (3)$$

To calculate the corrected biomass yields of R270 and R267 in the absence of increased glycerol formation ($Y_{xs}^{corr,\ glycerol}$), sucrose that was used for additional glycerol formation ($\Delta C_{s,glycerol}$) was subtracted from the total consumed sucrose ($C_{s,medium}$-$C_{s,residual}$) and biomass yields were calculated by Equation (4):

$$Y_{xs}^{corr,glycerol} = \left(\frac{C_x}{C_{s,medium} - C_{s,residual} - \Delta C_{s,glycerol}}\right) \quad (4)$$

5.2. Extracellular glucose-1-phosphate formation

Extracellular sucrose phosphorylation and subsequent uptake and anaerobic dissimilation of the resulting fructose results in a net yield of 2 mol ATP per 1 mol phosphorylated sucrose. The ATP 'lost' in the form of unused extracellular glucose-1-phosphate (G1P) can be represented in the form of sucrose not contributing to biomass formation ($\Delta C_{s,G1P}$). For R270 and R267, 1 mol of G1P formed is equivalent to 0.6 (3 out of 5 ATP lost) and 0.5 (2 out of 4 ATP lost) respectively, resulting in Equations (5) and (6):

$$\Delta C_{s,G1P^{R270}} = 0.6^* C_{G1P} \quad (5)$$

$$\Delta C_{s,G1P^{R267}} = 0.5^* C_{G1P} \quad (6)$$

To calculate the corrected biomass yields of R270 and R267 in the absence of extracellular sucrose phosphorolysis ($Y_{xs}^{corr,G1P}$), the calculated 'sucrose equivalent' that did not contribute to biomass formation ($\Delta C_{s,G1P}$ in mol l^{-1}) was subtracted from the total consumed sucrose ($C_{s,medium}$-$C_{s,residual}$) and biomass yields were calculated by Equation (7):

$$Y_{xs}^{corr,G1P} = \left(\frac{C_x}{C_{s,medium} - C_{s,residual} - \Delta C_{s,g1P}}\right) \quad (7)$$

5.3. Protein content

To quantify the impact of increased protein content in R270 and R267 compared to R249 (wt Mal11), an estimation of the ATP requirements for biomass formation of the three strains was made, based on a previous analysis of macromolecular composition and the corresponding energy requirements of yeast biomass (Supplementary Tables S5 and S6) (Stouthamer, 1973; Lange and Heijnen, 2001).

Variations in the protein content were observed between the strains used in this study, and we assumed that the ratio of the other (non-protein) macromolecules remained the same as was previously determined (Alexander, 1968), although their fraction of the total biomass decreased due to the increased protein content (Supplementary Table S6).

The ATP requirement for each component (ATP_i for component *i* in mmol g^{-1} component) (Supplementary Table S5) was then multiplied by the weight fraction of the corresponding component (γ_i in g g^{-1} biomass) to determine the total ATP requirement for biomass formation of each strain (ATP_x in mmol g_x^{-1}), including ATP requirements for mRNA turnover (ATP_{mRNA} in mmol g_x^{-1}) and transport of nutrients ($ATP_{transport}$ in mmol g_x^{-1}) via Equation (8):

$$ATP_x = \sum(ATP_i * \gamma_i) + ATP_{mRNA} + ATP_{transport} \quad (8)$$

To calculate the corrected biomass yields of R270 and R267 in a scenario in which their energetic cost of biomass synthesis would have been identical to R249 ($Y_{xs}^{corr,\ BioComp}$), the biomass yield of R270 was multiplied by the ratio of the ATP requirement of biomass synthesis of R270 (ATP_x^{R270}) or R267 (ATP_x^{R267}) over that of R249 (ATP_x^{R249}) Equation (9):

$$Y_{xs}^{corr,BioComp} = \left(\frac{C_x}{C_{s,medium} - C_{s,residual}}\right)^* \frac{ATP_X^{mutant}}{ATP_X^{R249}} \quad (9)$$

5.4. Final corrected biomass yields

To calculate the corrected biomass yields of R270 and R267 in the absence of additional glycerol and extracellular glucose-1-phosphate formation and with an identical protein content to R249, equations (4), (7) and (9) were combined in Equation (10):

$$Y_{xs}^{corr} = \left(\frac{C_x}{C_{s,medium} - C_{s,residual} - \Delta C_{s,glycerol} - \Delta C_{s,G1P}}\right)^* \frac{ATP_X^{mutant}}{ATP_X^{R249}} \quad (10)$$

CRediT authorship contribution statement

Ryan K. Henderson: Validation, Methodology, Formal analysis, Investigation, Writing - original draft. **Sophie C. de Valk:** Validation, Formal analysis, Investigation, Writing - original draft, Visualization. **Bert Poolman:** Conceptualization, Methodology, Formal analysis, Writing - review & editing, Supervision, Funding acquisition. **Robert Mans:** Conceptualization, Formal analysis, Writing - review & editing, Supervision, Project administration, Funding acquisition.

Acknowledgements

This work was carried out within the BE-Basic R&D Program, which was granted a FES subsidy from the Dutch Ministry of Economic affairs, agriculture and innovation (EL&I). The research was also funded by a NWO TOP-PUNT (project number 13.006) grant.

Appendix A. Supplementary data

Supplementary data to this article can be found online at https://doi.org/10.1016/j.ymben.2020.11.014.

References

Alexander, J.K., 1968. Purification and specificity of cellobiose phosphorylase from *Clostridium thermocellum*. J. Biol. Chem. 243, 2899–2904.

Arastu-Kapur, S., Arendt, C.S., Purnat, T., Carter, N.S., Ullman, B., 2005. Second-site suppression of a nonfunctional mutation within the *Leishmania donovani* inosine-guanosine transporter. J. Biol. Chem. 280, 2213–2219. https://doi.org/10.1074/jbc.M408224200.

Basso, T.O., et al., 2011. Engineering topology and kinetics of sucrose metabolism in *Saccharomyces cerevisiae* for improved ethanol yield. Metab. Eng. 13, 694–703. https://doi.org/10.1016/j.ymben.2011.09.005.

Belocopitow, E., Maréchal, L.R., 1970. Trehalose phosphorylase from *Euglena gracilis*. Biochim. Biophys. Acta 198, 151–154. https://doi.org/10.1016/0005-2744(70)90045-8.

van Bodegom, P., 2007. Microbial maintenance: a critical review on its quantification. Microb. Ecol. 53, 513–523. https://doi.org/10.1007/s00248-006-9049-5.

Borodina, I., Nielsen, J., 2014. Advances in metabolic engineering of yeast *Saccharomyces cerevisiae* for production of chemicals. Biotechnol. J. 9, 609–620. https://doi.org/10.1002/biot.201300445.

Brouwers, N., et al., 2018. *In vivo* recombination of *Saccharomyces eubayanus* maltose-transporter genes yields a chimeric transporter that enables maltotriose fermentation. PLoS Genet. 15 https://doi.org/10.1371/journal.pgen.1007853.

Canelas, A.B., et al., 2010. Integrated multilaboratory systems biology reveals differences in protein metabolism between two reference yeast strains. Nat. Commun. 1 https://doi.org/10.1038/ncomms1150.

van Dijken, J.P., Scheffers, W.A., 1986. Redox balances in the metabolism of sugars by yeasts. FEMS (Fed. Eur. Microbiol. Soc.) Microbiol. Rev. 32, 199–224. https://doi.org/10.1111/j.1574-6968.1986.tb01194.x.

Entian, K.-D., Kötter, P., 2007. Yeast genetic strain and plasmid collections. Methods Microbiol. 36, 629–666. https://doi.org/10.1016/S0580-9517(06)36025-4.

Gietz, R.D., Woods, R.A., 2002. Transformation of yeast by lithium acetate/single-stranded carrier DNA/polyethylene glycol method. Methods Enzymol. 350, 87–96. https://doi.org/10.1016/S0076-6879(02)50957-5.

de Groeve, M.R.M., et al., 2009. Creating lactose phosphorylase enzymes by directed evolution of cellobiose phosphorylase. Protein Eng. Des. Sel. 22, 393–399. https://doi.org/10.1093/protein/gzp017.

Guimarães, P.M.R., Londesborough, J., 2008. The adenylate energy charge and specific fermentation rate of brewer's yeasts fermenting high- and very high-gravity worts. Yeast 25, 47–58. https://doi.org/10.1002/yea.1556.

Han, E.-K., Cotty, F., Sottas, C., Jiang, H., Michels, C.A., 1995. Characterization of *AGT1* encoding a general α-glucoside transporter from *Saccharomyces*. Mol. Microbiol. 17, 1093–1107. https://doi.org/10.1111/j.1365-2958.1995.mmi_17061093.x.

Henderson, R.K., Poolman, B., 2017. Proton-solute coupling mechanism of the maltose transporter from *Saccharomyces cerevisiae*. Sci. Rep. 7 https://doi.org/10.1038/s41598-017-14438-1.

Henderson, R.K., Fendler, K., Poolman, B., 2019. Coupling efficiency of secondary active transporters. Curr. Opin. Biotechnol. 58, 62–71. https://doi.org/10.1016/j.copbio.2018.11.005.

Hong, K.-K., Hou, J., Shoaie, S., Nielsen, J., Bordel, S., 2012. Dynamic 13C-labeling experiments prove important differences in protein turnover rate between two *Saccharomyces cerevisiae* strains. FEMS Yeast Res. 12, 741–747. https://doi.org/10.1111/j.1567-1364.2012.00823.

Horák, J., 2013. Regulations of sugar transporters: insights from yeast. Curr. Genet. 59, 1–31. https://doi.org/10.1007/s00294-013-0388-8.

Jessen-Marshall, A.E., Parker, N.J., Brooker, R.J., 1997. Suppressor analysis of mutations in the loop 2-3 motif of lactose permease: evidence that glycine-64 is an important residue for conformational changes. J. Bacteriol. 179, 2616–2622. https://doi.org/10.1128/jb.179.8.2616-2622.1997.

Kim, H., Lee, W.-H., Galazka, J.M., Cate, J.H.D., Jin, Y.-S., 2014. Analysis of cellodextrin transporters from *Neurospora crassa* in *Saccharomyces cerevisiae* for cellobiose fermentation. Appl. Microbiol. Biotechnol. 98, 1087–1094. https://doi.org/10.1007/s00253-013-5339-2.

de Kok, S., et al., 2011. Increasing free-energy (ATP) conservation in maltose-grown *Saccharomyces cerevisiae* by expression of a heterologous maltose phosphorylase. Metab. Eng. 13, 518–526.

de Kok, S., Kozak, B.U., Pronk, J.T., van Maris, A.J.A., 2012. Energy coupling in *Saccharomyces cerevisiae*: selected opportunities for metabolic engineering. FEMS Yeast Res. 12, 387–397. https://doi.org/10.1111/j.1567-1364.2012.00799.x.

Lange, H.C., Heijnen, J., 2001. J. Statistical reconciliation of the elemental and molecular biomass composition of *Saccharomyces cerevisiae*. Biotechnol. Bioeng. 75, 334–344. https://doi.org/10.1002/bit.10054.

Van Leeuwen, C.C.M., Weusthuis, R.A., Postma, E., Van den Broek, P.J.A., Van Dijken, J. P., 1992. Maltose/proton co-transport in *Saccharomyces cerevisiae*. Comparative study with cells and plasma membrane vesicles. Biochem. J. 284, 441–445. https://doi.org/10.1042/bj2840441.

Lolkema, J.S., Poolman, B., 1995. Uncoupling in Secondary Transport Proteins. A mechanistic explanation for mutants of *lac* permease with an uncoupled phenotype. J. Biol. Chem. 270, 12670–12676. https://doi.org/10.1074/jbc.270.21.12670.

Luttik, M.A., et al., 2000. The *Saccharomyces cerevisiae ICL2* gene encodes a mitochondrial 2-methylisocitrate lyase involved in propionyl-coenzyme A metabolism. J. Bacteriol. 182, 7007–7013. https://doi.org/10.1128/JB.182.24.7007-7013.2000.

Mans, R., Daran, J.-M.G., Pronk, J.T., 2018. Under pressure: evolutionary engineering of yeast strains for improved performance in fuels and chemicals production. Curr. Opin. Biotechnol. 50, 47–56. https://doi.org/10.1016/j.copbio.2017.10.011.

van Maris, A.J.A., Winkler, A.A., Porro, D., van Dijken, J.P., Pronk, J.T., 2004. Homofermentative lactate production cannot sustain anaerobic growth of engineered *Saccharomyces cerevisiae*: possible consequence of energy-dependent lactate export. Appl. Environ. Microbiol. 70, 2898–2905.

Marques, W.L., Raghavendran, V., Stambuk, B.U., Gombert, A.K., 2015. Sucrose and *Saccharomyces cerevisiae*: a relationship most sweet. FEMS Yeast Res. 16 https://doi.org/10.1093/femsyr/fov107.

Marques, W.L., et al., 2018a. Combined engineering of disaccharide transport and phosphorolysis for enhanced ATP yield from sucrose fermentation in *Saccharomyces cerevisiae*. Metab. Eng. 45, 121–133. https://doi.org/10.1016/j.ymben.2017.11.012.

Marques, W.L., et al., 2018b. Laboratory evolution and physiological analysis of *Saccharomyces cerevisiae* strains dependent on sucrose uptake via the *Phaseolus vulgaris* Suf1 transporter. Yeast 35, 639–652. https://doi.org/10.1002/yea.3357.

Pao, S.S., Paulsen, I.T., Saier, M.H., 1998. J. Major Facilitator Superfamily. Microbiol. Mol. Biol. Reviews 62, 1–34. https://doi.org/10.1128/MMBR.62.1.1-34.1998.

Pazdernik, N.J., Cain, S.M., Brooker, R.J., 1997. An analysis of suppressor mutations suggests that the two halves of the lactose permease function in a symmetrical manner. J. Biol. Chem. 272, 26110–26116. https://doi.org/10.1074/jbc.272.42.26110.

Pfromm, P.H., Amanor-Boadu, V., Nelson, R., Vadlani, P., Madl, R., 2010. Bio-butanol vs. bio-ethanol: a technical and economic assessment for corn and switchgrass fermented by yeast or *Clostridium acetobutylicum*. Biomass Bioenergy 34, 515–524.

Pi, J., Chow, H., Pittard, A.J., 2002. Study of second-site suppression in the *pheP* gene for the phenylalanine transporter of *Escherichia coli*. J. Bacteriol. 184, 5842–5847. https://doi.org/10.1128/JB.184.21.5842-5847.2002.

Quistgaard, E.M., Löw, C., Guettou, F., Nordlund, P., 2016. Understanding transport by the major facilitator superfamily (MFS): structures pave the way. Nat. Rev. Mol. Cell Biol. 17 https://doi.org/10.1038/nrm.2015.25.

van Rossum, H.M., Kozak, B.U., Pronk, J.T., van Maris, A.J.A., 2016. Engineering cytosolic acetyl-coenzyme A supply in *Saccharomyces cerevisiae*: pathway stoichiometry, free-energy conservation and redox-cofactor balancing. Metab. Eng. 36, 99–115. https://doi.org/10.1016/j.ymben.2016.03.006.

Sadie, C.J., Rose, S.H., den Haan, R., van Zyl, W.H., 2011. Co-expression of a cellobiose phosphorylase and lactose permease enables intracellular cellobiose utilisation by *Saccharomyces cerevisiae*. Appl. Microbiol. Biotechnol. 90, 1373–1380.

Salazar, A.N., et al., 2017. Nanopore sequencing enables near-complete de novo assembly of *Saccharomyces cerevisiae* reference strain CEN.PK113-7D. FEMS Yeast Res. 17, 1–11. https://doi.org/10.1093/femsyr/fox074.

Saraceni-Richards, C.A., Levy, S.B., 2000. Second-site suppressor mutations of inactivating substitutions at Gly247 of the tetracycline efflux protein, tet(B). J. Bacteriol. 182, 6514–6516. https://doi.org/10.1128/JB.182.22.6514-6516.2000.

Serrano, R., 1977. Energy requirements for maltose transport in yeast. Eur. J. Biochem. 80, 97–102. https://doi.org/10.1111/j.1432-1033.1977.tb11861.x.

Sheth, K., Alexander, J.K., 1967. Cellodextrin phosphorylase from *Clostridium thermocellum*. Biochim. Biophys. Acta 148, 808–810. https://doi.org/10.1016/0304-4165(67)90057-8.

Stambuk, B.U., de Araujo, P.S., 2001. Kinetics of active α-glucoside transport in *Saccharomyces cerevisiae*. FEMS Yeast Res. 1, 73–78. https://doi.org/10.1111/j.1567-1364.2001.tb00015.x.

Stouthamer, A.H., 1973. A theoretical study on the amount of ATP required for synthesis of microbial cell material. Antonie Leeuwenhoek 39, 545–565. https://doi.org/10.1007/BF02578899.

Verduyn, C., Postma, E., Scheffers, W.A., van Dijken, J.P., 1990. Physiology of *Saccharomyces cerevisiae* in anaerobic glucose-limited chemostat cultures. J. Gen. Microbiol. 136, 395–403. https://doi.org/10.1099/00221287-136-3-395.

Yan, N., 2015. Structural biology of the major facilitator superfamily transporters. Annu. Rev. Biophys. 44, 257–283. https://doi.org/10.1146/annurev-biophys-060414-033901.

Zelle, R.M., et al., 2008. Malic acid production by *Saccharomyces cerevisiae*: engineering of pyruvate carboxylation, oxaloacetate reduction, and malate export. Appl. Environ. Microbiol. 74, 2766–2777.

Zhou, Y., Qu, H., Dibley, K.E., Offler, C.E., Patrick, J.W., 2007. A suite of sucrose transporters expressed in coats of developing legume seeds includes novel pH-independent facilitators. Plant J. 49, 750–764.